Real-Time Noninvasive Imaging of Fatty Acid Uptake *in Vivo*

Amy H. Henkin,[†,¶] Allison S. Cohen,[‡,¶] Elena A. Dubikovskaya,[‡,⊥,¶] Hyo Min Park,[†] Gennady F. Nikitin,[⊥] Mathieu G. Auzias,[⊥] Melissa Kazantzis,[†] Carolyn R. Bertozzi,[‡,§,‖] and Andreas Stahl*,[†]

Departments of [†]Nutritional Science and Toxicology, [‡]Chemistry, and [§]Molecular and Cell Biology and [‖]Howard Hughes Medical Institute, University of California Berkeley, Berkeley, California 94720, United States

[⊥]Institute of Chemical Sciences and Engineering, École Polytechnique Fédérale de Lausanne, LCBIM, 1015 Lausanne, Switzerland

Ⓢ *Supporting Information*

ABSTRACT: Detection and quantification of fatty acid fluxes in animal model systems following physiological, pathological, or pharmacological challenges is key to our understanding of complex metabolic networks as these macronutrients also activate transcription factors and modulate signaling cascades including insulin sensitivity. To enable noninvasive, real-time, spatiotemporal quantitative imaging of fatty acid fluxes in animals, we created a bioactivatable molecular imaging probe based on long-chain fatty acids conjugated to a reporter molecule (luciferin). We show that this probe faithfully recapitulates cellular fatty acid uptake and can be used in animal systems as a valuable tool to localize and quantitate in real time lipid fluxes such as intestinal fatty acid absorption and brown adipose tissue activation. This imaging approach should further our understanding of basic metabolic processes and pathological alterations in multiple disease models.
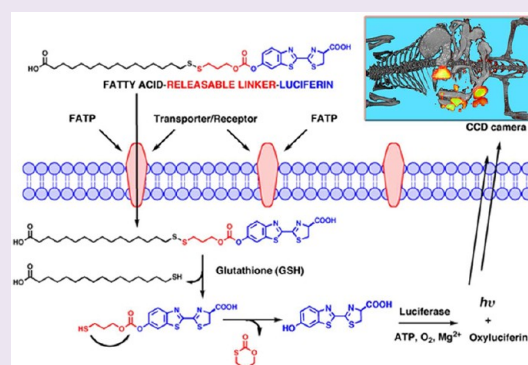
The uptake of lipids such as free fatty acids (FFAs) is altered under several physiological and pathological conditions, reflecting important underlying metabolic processes such as fasting and cold activation of brown adipose tissue (BAT),[1] as well as pathologies including cardiac hypoxia[2] and intestinal malabsorption.[3] Excessive uptake of FFAs has also been linked to insulin resistance in skeletal muscle,[4] cardiac myopathies,[5] hepatosteatosis,[6] and lipotoxicity in heart,[7] liver,[8] and pancreatic β-cells.[9] Further, FFA/lipid fluxes are altered by pharmacological interventions as part of the drug's mode of action, as in the case of the anti-diabetic glitazones, which enhance FFA uptake and sequestration by adipocytes,[10] or the anti-obesity compound orlistat, which blocks the generation of FFAs from triglycerides in the intestine.[11] Changes in fatty acid uptake and utilization can also occur as an unwanted side effect of pharmacological intervention as exemplified by the anti-cancer drug doxorubicin, which causes cardiac metabolic remodeling.[12] Thus, localizing and quantifying changes in fatty acid uptake in particular and lipid flux in general has wide implications not only for fundamental biological studies but also for the diagnosis of diseases, the evaluation of novel treatment approaches, and for drug discovery.

Existing technologies for the *in vivo* imaging of fatty acids have primarily relied on positron emission tomography (PET) and single-photon emission computed tomography (SPECT) probes.[13,14] However, these imaging technologies suffer from several shortcomings including the use of ionizing radiation. The main FFA PET probe has been ^{11}C-palmitate, which has the major advantage of reflecting the metabolic kinetics of unlabeled palmitate and has been primarily used for the

imaging of cardiac lipid metabolism.[13] However, due to a very short half-life (~20 min), generation of ^{11}C-palmitate requires an onsite cyclotron, making it unsuitable to image processes, such as intestinal lipid absorption, that occur on the order of hours.[15] Further, ^{11}C-palmitate is quickly metabolized to [11]CO$_2$, leading to reduced image quality. These problems led to the development of ^{18}F-labeled fatty acid analogues, such as 14-(R,S)-^{18}F-fluoro-6-thiaheptadecanoic acid (FTHA),[16] that are trapped inside of cells and offer marginally longer half-lifes (~110 min). However, it was later found that FTHA uptake was likely to reflect unphysiological processes, as it was insensitive to inhibition of β-oxidation.[17] These limitations and associated high costs have limited the usefulness of PET and SPECT for clinical and preclinical studies of fatty acid fluxes *in vivo*, resulting in a virtual absence of spatiotemporal imaging reports of important physiological processes such as intestinal lipid absorption. In contrast, bioluminescence imaging (BLI) is a highly sensitive preclinical *in vivo* imaging modality[18−20] that has found use in oncology as well as the quantitative imaging of gene[19,21] and enzyme activities such as caspases,[22,23] β-lactamases,[24] furins,[25] and β-galactosidase,[26] the imaging of protein−protein interactions,[21] and the imaging of fluxes of hydrogen peroxide.[27]

Here, we describe an approach that overcomes the major deficiencies of classical methodologies and relies on a sensitive
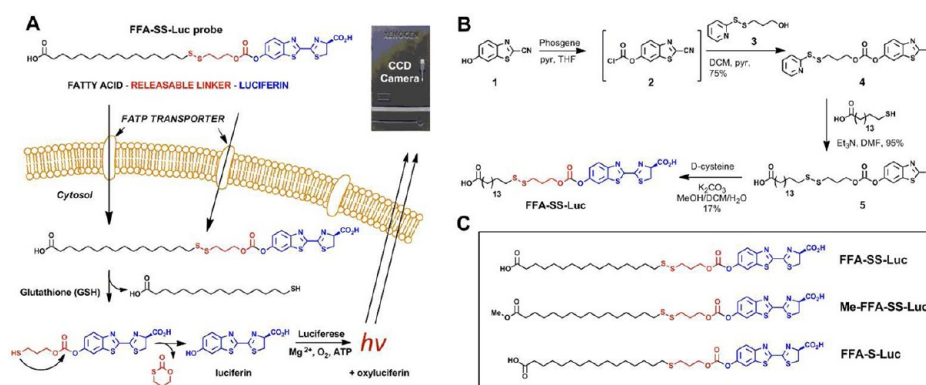
Figure 1. Molecular probes for bioluminescent *in vivo* imaging of fatty acid uptake. (a) Strategy for bioluminescence imaging of fatty acid uptake. The compound is taken up by a transporter-mediated process. The disulfide bond is reduced by intracellular glutathione, and the resultant thiol undergoes cyclization releasing free luciferin. Luciferase-catalyzed conversion of luciferin to oxyluciferin is accompanied by production of a photon of light, which is detected using a charge-coupled device (CCD) camera (IVIS Spectrum, PerkinElmer, CA). (b) Synthesis of FFA-SS-luc. 2-Cyano-6-hydroxybenzothiazole **1** is converted *in situ* into the chloroformate **2** by reaction with a solution of phosgene. In a separate route, 3-mercapto-1-propanol is transformed with 2'-aldrithiol to 3-(pyridin-2-yldisulfanyl)propan-1-ol (**3**), an activated disulfide, according to a previously published procedure.[30] *In situ* coupling of compound **3** with chloroformate **2** provided carbonate **4**. The thiopyridyl moiety of **4** was displaced with 16-mercaptohexadecanoic acid to give the fatty acid-linker conjugate **5**. Condensation with D-cysteine completed the D-luciferin scaffold, resulting in the desired FFA-SS-luc probe. (c) Structures of fatty acid probe (FFA-SS-luc) and control imaging compounds (Me-FFA-SS-luc and FFA-S-luc). Fatty acid is shown in black, linker is shown in red, and luciferin is shown in blue. FFA: fatty acid; SS: disulfide bond necessary for intracellular linker release upon uptake into cells *via* FFA transporters; S: thioether bond that serves as a control for background hydrolysis; Me: methyl ester that serves as the control for passive diffusion inside the cells; luc: luciferin.

and highly quantitative BLI to enable fundamental imaging studies of lipid metabolism in disease models.

RESULTS AND DISCUSSION

Concept and Design of FFA-SS-luc. The general concept of our approach is to attach the optical imaging probe luciferin to a long-chain fatty acid *via* a cleavable disulfide bond that is stable in the extracellular environment but readily reduces intracellularly after lipid uptake (Figure 1a). The synthesis scheme for the probe, termed FFA-SS-luc, is outlined in Figure 1b and detailed in the Supporting Information. The design of FFA-SS-luc was based on several considerations. First, the probe should be taken up by the same physiological transport process as natural fatty acids. On the basis of our prior knowledge of fatty acid transporter (FATP) substrate specificity,[28] we selected a >10 carbon, even numbered, unbranched and non-esterified FFA as a lipid probe. The fatty acid was connected *via* a disulfide linker to luciferin as these linkers have been shown to be stable outside of cells following injections into animals.[29−31] We choose to utilized a non-toxic probe that only upon liberation from the linker generates a signal by taking advantage of the fact that luciferin derivatives alkylated on the phenolic oxygen do not generate light.[32] Thus, free luciferin is generated and subsequently quantified following disulfide linker reduction that leads to instantaneous cyclization of the linker. Free luciferin is then converted by luciferase to oxyluciferin and a photon of light[33] (Figure 1a). This facilitates real-time noninvasive detection of FFA uptake using bioluminescent imagers with an excellent signal-to-background ratio and the possibility of spatial localization of signal generating organs (IVIS Spectrum, PerkinElmer, CA) As controls, we also synthesized a methyl ester of FFA-SS-luc, termed Me-FFA-SS-luc (Figure 1c), which should not be a substrate for FFA transporters[28] because the carboxylic acid of the FFA part is methylated (Figure 1c).

As a control for nonspecific hydrolysis of the carbonate part of the linker, we also prepared a thioether analogue of the FFA-

SS-probe (FFA-S-luc probe, Figure 1c). The only difference between this control compound and the FFA-SS-luc probe is the absence of the disulfide bond that would produce free luciferin specifically upon entry into the cell. The control compound can be hydrolyzed inside or outside the cell with subsequent release of free luciferin upon cleavage of the carbonate bond. We further confirmed that the background hydrolysis of the probes is negligible during the course of the experiment by showing that spontaneous generation rates of free luciferin from the FFA-SS-luc probe translate into a half-life of 432 min (7.2 h) (Supplementary Figure S1).

***In Vitro* Validation of FFA-SS-luc.** To determine the physiological parameters of cellular uptake, we generated a firefly luciferase expressing stable cell line termed 3T3-luc based on 3T3 L1 cells that can be readily differentiated from a fibroblast precursor to a terminally differentiated adipocyte. To test uptake of the new compound by 3T3-luc fibroblasts and adipocytes, cells were seeded into 96-well plates and incubated with bovine serum albumin (BSA)-bound FFA-SS-luc at various concentrations while light emission was being monitored with a bioluminescent imaging system (Figure 2a). Comparison of 3T3-luc adipocytes and fibroblasts showed much more robust uptake rates of the fatty acid compound by the differentiated cells (Figure 2b), which is in line with previous reports based on radio- and fluorescent-labeled fatty acids.[34] Further, 3T3-luc adipocytes showed a dose-dependent increase in uptake rates in the concentration range from 0−100 μM (Figure 2c). To further demonstrate that uptake of the novel fatty acid imaging compound occurs *via* physiological mechanisms, we compared uptake of FFA-SS-luc by 3T3-luc adipocytes with Me-FFA-SS-luc (Figure 1c and Supplementary Scheme S1) and luciferin. Both Me-FFA-SS-luc and unconjugated free luciferin showed significantly lower uptake rates in adipocytes compared to FFA-SS-luc (Figure 3a). Most importantly, we were able to inhibit FFA-SS-luc uptake by adipocytes with an excess of oleate (Figure 3b), but not methyloleate (Figure 3c), demonstrating that the uptake process for
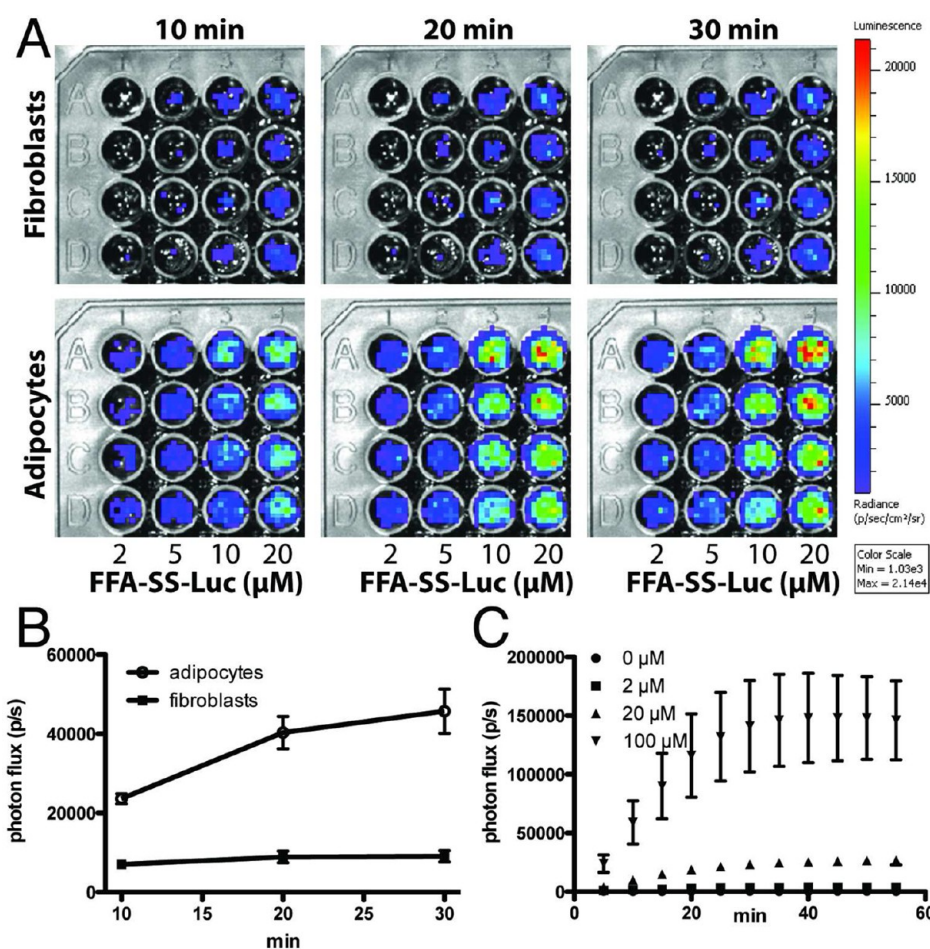
Figure 2. FFA-SS-luc uptake by 3T3-luc adipocytes and fibroblasts. (a) Image overlay of a photographic image and bioluminescence from 96-well plates containing equal number of 3T3-luc fibroblasts (upper row) or adipocytes (lower row) incubated with the indicated concentrations of FFA-SS-luc for 10, 20, and 30 min. Scale min: 1.03×10^3 and max: 2.14×10^4 p/s (photons/second). (b) Uptake of 20 μM FFA-SS-luc by luciferase expressing undifferentiated 3T3 L1 fibroblasts or adipocytes ($n = 4$) over 30 min. Results are expressed as mean $\pm$ SD. (c) Uptake kinetics of FFA-SS-luc at the indicated concentrations by 3T3-L1 adipocytes. Error bars represent the standard deviation of the mean of $n = 8$ data points.

the imaging compound overlaps with that of natural fatty acid substrates.

While circulating long-chain fatty acids are bound to albumin, dietary lipid absorption occurs in the context of fatty acid/bile acid mixed micelles. To interrogate whether FFA-SS-luc could also be used to image this important physiological process, we created FFA-SS-luc/taurocholate mixed micelles as reported before using fluorescent fatty acids[28] and incubated them with primary enterocytes from the duodenum of luciferase-expressing FVB-luc⁺ mice.[35] Enterocytes produced a dose-dependent signal following incubation with FFA-SS-luc/taurocholate mixed micelles (data not shown), and importantly, uptake of FFA-SS-luc could be robustly competed with an excess of either palmitate or oleate (Figure 3d), the two predominant long-chain fatty acids in the human diet.

To further demonstrate that uptake of FFA-SS-luc by cells is indeed associated with specific protein interactions on the cell surface rather than unspecific processes, such as pinocytosis, we determined the uptake rates of albumin-bound FFA-SS-luc by HEK293 cells, which stably express the hepatic fatty acid transporter FATP5.[36] Using fluorescent and radio-labeled fatty acids we have previously demonstrated that FATP5 expression robustly enhances cellular fatty acid uptake compared to vector controls.[37] Following transient transfection of control and

FATP5 cells with firefly luciferase we were able to detect a 7.3 times higher signal in the FATP5 expressing cells versus controls (Figure 3e). This difference did not significantly change and remained highly significant (6.25 times increase, $p <$ 0.001) even after correcting for transfection efficiency using the luciferin signal (Figure 3e insert).

Physiological uptake of FFA-SS-luc was further supported by reproducing the known stimulatory effect of insulin on FFA uptake.[38] We were able to monitor changes in FFA uptake rates in real time immediately following insulin addition (Figure 3f). Notably, the use of BLI, unlike other imaging methods, permitted monitoring of both signal increase and dissipation. The noncumulative nature of the light signal generated upon uptake allowed us to clearly detect the uptake kinetics of FFA in the presence or absence of insulin. By contrast, traditional fluorescence- or radio-imaging methods[39] produce signals that accumulate over time and thus make the detection of dynamic changes accompanying prolonged imaging more challenging.

***In Vivo* Imaging of Intestinal Fatty Acid Uptake Using FFA-SS-luc.** Having validated FFA-SS-luc in cultured adipocytes, we next tested its capabilities in mice expressing luciferase under the control of the actin promoter (FVB-luc⁺) (Figures 4 and 5).[35] Oral delivery of FFA-SS-luc using cremophor, poly(ethylene glycol) (PEG 400), and 1:1 mixtures of PEG/
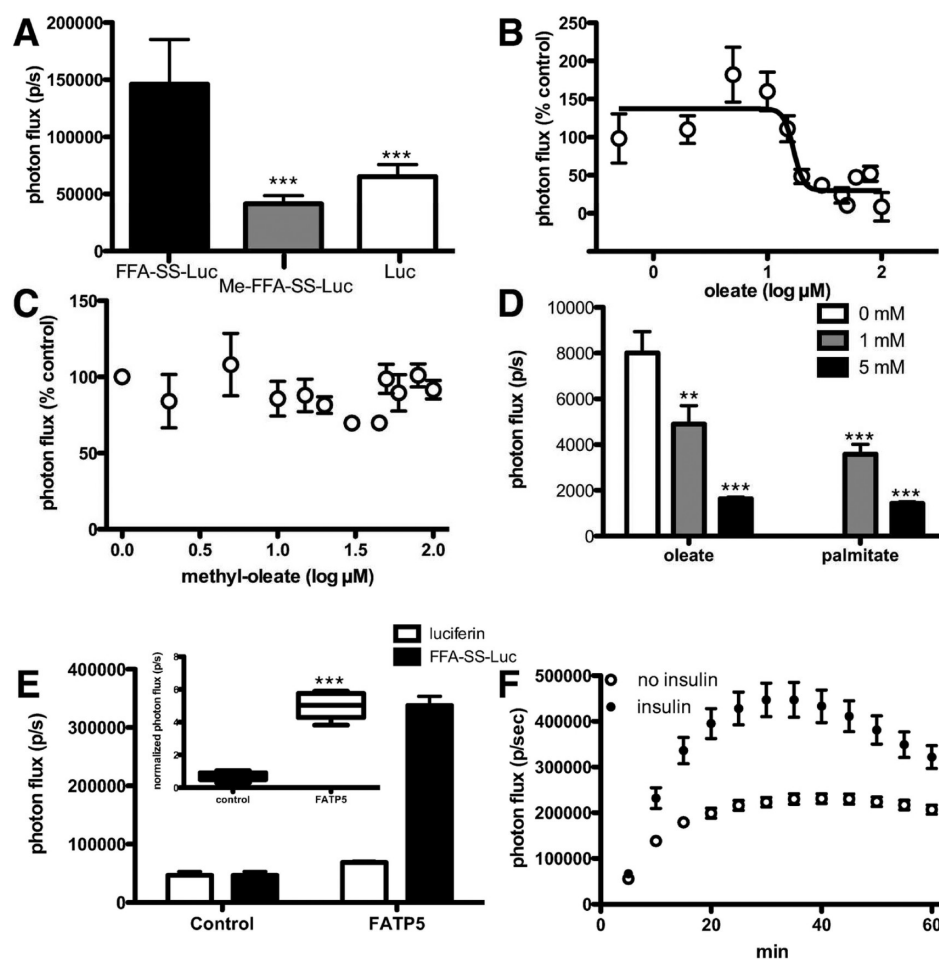
Figure 3. Characterization of fatty acid probe uptake *in vitro*. (a) Uptake rate of FFA-SS-luc, Me-FFA-SS-luc, and luciferin (each at 20 μM) over a 30 min time course; $n = 8$. (b) Concentration-dependent inhibition curve of oleate against uptake of 20 μM FFA-SS-luc by 3T3-L1 adipocytes (IC$_{50}$ = 17 μM). Error bars represent the standard deviation of the mean of $n = 8$ data points. (c) As in panel b, but with methyl-oleate; $n = 8$. (d) Competition of FFA-SS-luc (150 μM) uptake from taurocholate mixed micelles with the indicated concentrations of oleate and palmitate using luciferase expressing primary enterocytes. (e) Light emission from vector controls and hsFATP5 expressing HEK293 cells incubated with luciferin or FFA-SS-luc following transient transfection with luciferase. Insert shows FFA-SS-luc signal normalized to luciferin to correct for transfection efficiency. (f) Uptake kinetics of 20 μM FFA-SS-luc by 3T3-L1 adipocytes with or without a preincubation with 1 μg mL^{-1} insulin; $n = 8$. Results are expressed as mean $\pm$ SD. ** $p < 0.01$; *** $p < 0.001$.

propylene glycol (PG) as delivery vehicles all showed an abdominal signal as shown in Figure 4a with uptake kinetics that slowly increased over the time frame of hours (Supplementary Figure S2 and Movie S1), in line with expected kinetics of intestinal FFA absorption.[15] To verify that the signal was indeed emanating from the small intestine, we performed multimodal imaging with BLI and computed tomography (CT) utilizing barium sulfate as a contrast reagent to highlight the gastrointestinal (GI) tract (Figure 4b). Co-registered overlays of the CT and BLI images (following 3D localization of the signal with diffuse luminescent imaging tomography[40]) show that the signal generated by FFA-SS-luc is indeed in the small intestine (Figure 4b). This was further confirmed by excising the GI tract from the stomach to the colon. Importantly, the strongest signal was generated by the proximal duodenum (Figure 4c, 2), while the stomach (Figure 4c, 1) and colon (Figure 4c, 3) were negative. This observation is in excellent agreement with the known pattern of long-chain fatty acid absorption in murine and human intestine[41] and highlights the specificity of uptake, as the stomach is negative despite receiving the largest dose of FFA-SS-luc. These

experiments demonstrate the utility of this technique for the molecular imaging of fatty acid uptake by the intestine in a living mammal and should enable the testing of dietary and pharmacological interventions aimed at blocking or delaying fatty acid absorption to reduce caloric uptake and maximize incretin secretion.[42]

We further validated the mechanism of BLI generated by using the FFA-SS-luc control compound FFA-S-luc (Figure 1c and Supplementary Scheme S2), which lacks a cleavable linker and instead includes a thioether bond. Using the same procedures as with FFA-SS-luc, we only observed a weak and diffuse signal upon oral gavage of the control compound (Figure 4d).

Further *in Vivo* Imaging Applications of FFA-SS-luc: Imaging of the Adipose Tissue, Liver, Kidneys, Heart, and Skeletal Muscle. To further demonstrate the versatility of the method, FFA-SS-luc (20 μM) was bound to 0.1% BSA and injected intravenously into the tail vein of FVB-luc$^+$ mice followed immediately by BLI. FFA-SS-luc rapidly generated strong signals from the upper body cavity and the leg musculature (Figure 5a). As expected for a natural long-chain
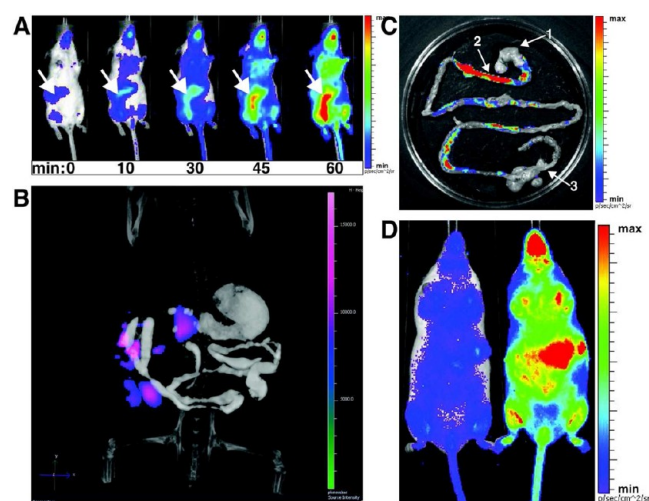
Figure 4. Uptake of FFA-SS-luc by the small intestine in FVB-luc[+] mice. (a) Ventral luminescent/photographic overlay sequence of animals following a gavage with 100 μL FFA-SS-luc (20 μM) in cremophor. Scale min: 1.64×10^5 p/s and max: 2.60×10^6 p/s (photons/second). (b) Luminescent/μCT overlay of FFA-SS-luc uptake by the small intestine following two barium sulfate administrations (80 mg each over 1 h) and gavage with 50 μL of FFA-SS-luc (300 μM) in 1:1 PEG 400 and PG. Bioluminescent signal was imaged for 1 h followed immediately by a μCT scan. 3D data sets from both imaging modalities were overlaid using Living Image 4.1 software. (c) Luminescent/photographic overlay of excised GI tract 1 h after gavage with 50 μL of a 300 μM FFA-SS-luc (0.01 mg) solution in 1:1 PEG 400 and PG. Scale min: 9.8×10^4 p/s and max: 3.37×10^5 p/s. Numbers indicate 1: stomach; 2: duodenum; 3: colon. (d) Ventral luminescent/photographic overlay comparing the BLI of FFA-SS-luc (right) and the control FFA-S-luc (left) 20 min postgavage. Mice were gavaged with 50 μL of a 300 μM solution of either compound (0.01 mg) in 1:1 PEG 400 and PG. Scale min: 3.74×10^3 p/s and max: 4.52×10^4 p/s.

fatty acid, FFA-SS-luc was taken up by several organs as confirmed *ex vivo*. Particularly, the adipose tissue, liver, kidneys, heart, and skeletal muscle generated strong signals (Figure 5b, I–V) in line with known fuel and FFA uptake preferences.[43] Using the actin promoter luciferase transgenic mice,[35] we were able to detect a robust BLI signal from the BAT area (see arrows in Figure 5c) that increased in intensity over the initial 20 min post intraperitoneal injection of FFA-SS-luc (Figure 5d and Supplementary Movie S2). Excision of the BAT confirmed that the signal in the interscapular area was indeed emanating from the BAT pads (Figure 5c, IV–VI). Contrarily, injection of FFA-S-luc generated little or no signal from intact (Figure 5c, I) or excised (Figure 5c, IV) BAT, thus confirming the specificity of our imaging reagent.

We previously showed that β-adrenergic agonists enhance FFA uptake by BAT in a FATP1-dependent fashion.[1] Importantly, injection of the β-3 adrenergic agonist CL316,243 led to a highly reproducible and significant increase in FFA-SS-luc uptake by BAT (Figure 5c, II/V vs III/VI). The CL316,243-induced changes in BAT BLI were highly reproducible in a cohort of 16 animals (Figure 5d). This demonstrates that we are able to quantitate physiologically meaningful changes in the spatiotemporal flux of fatty acids in real time using live animals.

In summary, FFA-SS-luc enables the interrogation of FFA uptake of internal organs in real time using live animals with the potential ability to further restrict signal through tissue-specific
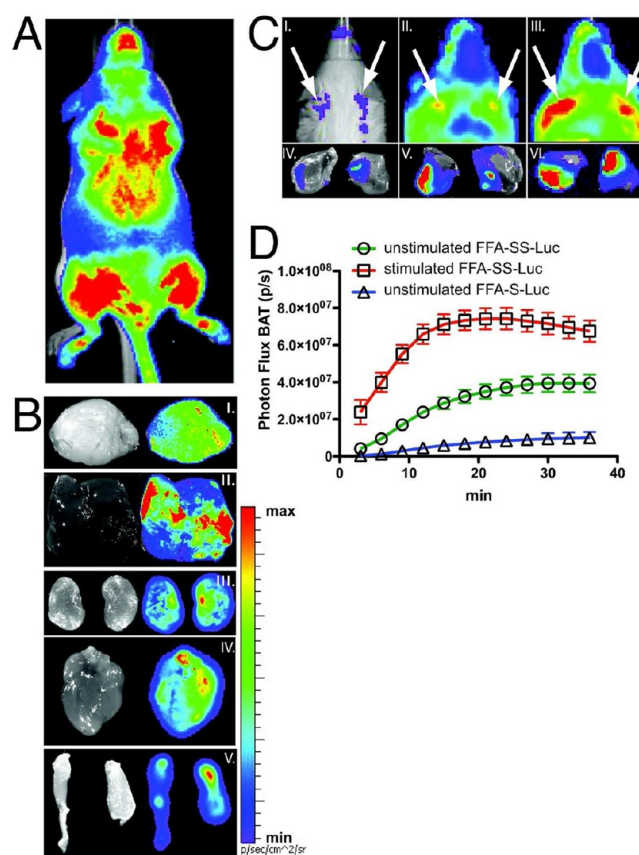

Figure 5. Uptake of FFA-SS-luc following injection into FVB-luc[+] mice. (a) Ventral luminescent/photographic overlay of mouse 5 min after tail vein injection of FFA-SS-luc (100 μL of a 20 μM solution bound to 0.1% BSA in PBS). Scale min: 8.04×10^3 p/s and max: 1.54×10^5 p/s (photons/second). (b) Luminescent/photographic overlay of FFA-SS-luc uptake by (I) white adipose tissue (WAT), (II) liver, (III) kidneys, (IV) heart, and (V) skeletal muscle, excised from FVB-luc[+] mice 5 min after FFA-SS-luc administration as in panel a. (c) Ventral luminescent/photographic overlay of intact (I–III) and excised (IV–VI) BAT 30 min after intraperitoneal (IP) injection of 100 μL of a 0.1% (w/v) BSA PBS solution containing either 200 μM FFA-S-luc (I/IV), FFA-SS-luc (II/V), or FFA-SS-luc with 1 mg/kg of the β-adrenergic agonist CL316243 (III/VI). I–III scale min: 2.62×10^5 p/s and max: 5.02×10^6 p/s. IV–VI scale min: 1.85×10^4 p/s and max: 8.34×10^5 p/s. (d) BAT uptake kinetics of FFA-S-luc (blue triangles, $N = 6$ animals), FFA-SS-luc (green circles, $N = 12$ animals), and FFA-SS-luc + 1 mg/kg CL316243 (red squares, $N = 16$ animals). All compounds were administered as stated in panel c. BLI images were acquired every 3 min immediately after compound administration. FFA uptake rate by BAT was calculated by drawing regions of interest around the interscapular region of each mouse. Error bars represent the standard deviation.

luciferase expression. BLI imaging with FFA-SS-luc enables quantitative spatiotemporal analysis of FFA uptake associated with important physiological processes. Notably, the technique allows *in vivo* monitoring of FFA uptake by the small intestine and BAT in real time in live animals. Since both processes are of significant importance to human health, this new technology opens a wide range of opportunities for establishment of new drug screens and investigations of fundamental biological processes involving FFA absorption and distribution. For example, blocking intestinal lipid absorption could reduce caloric uptake,[11] and shifting the absorption of dietary fatty acids to the distal small intestine could stimulate incretin

release and thus decrease feeding while enhancing insulin sensitivity.[42] Activation of fatty acid oxidation by BAT could be used for novel anti-obesity approaches.[44] Quantifying changes in fatty acid uptake has wide implications for fundamental biological observations as well as the diagnosis of diseases, evaluation of novel treatment approaches, and drug discovery. Finally, the design principles embodied in FFA-SS-luc can be extended to probes for the uptake of triglycerides and other lipids and the development of such technologies is currently on the way in our laboratories.

■ METHODS

Synthesis of Compounds. Unless otherwise stated, all reagents and solvents were obtained from commercial sources and used without purification. The synthesis of compounds is described in detail in the Supporting Information.

Luciferase Expressing Cellular Model (3T3-L1-luc Cells). 3T3-L1 fibroblasts (ATCC) were stably transfected with the pGL4.51-[luc2/CMV/Neo] vector (Promega). Clones with the highest level of luciferase expression were isolated and expanded.

Cell Culture and Treatment. 3T3-L1-luc fibroblasts were grown in DMEM containing 10% (v/v) fetal bovine serum with 2 mM L-glutamine and 1% (v/v) penicillin/streptomycin (DMEM/FBS). A cell differentiation protocol was followed as previously described.[45] For additional details, see the Supporting Information.

Animal Models. Transgenic mice ubiquitously expressing luciferase under control of the actin promoter (FVB-luc+ [FVB-Tg(CAG-luc,-GFP)L2G85Chco/J] mice) were kindly provided by Dr. Contag at Stanford University.[35] All animal studies were approved by and performed according to the guidelines of the Animal Care and Use Committee of the University of California, Berkeley.

Imaging Equipment and Software. All luminescent/photographic images were captured with the IVIS Spectrum (Caliper Life Sciences). Photon flux (photons/second) of regions of interest were calculated with the IVIS Living Image software. CT data were acquired with the Quantum FX μCT (Caliper Life Sciences) and superimposed with BLI data using Living Image.

Cell-Based Fatty Acid Uptake Assays. 3T3-luc adipocytes or fibroblasts were seeded into black-wall/clear-bottom-96-well plates (Costar) and treated with 100 μL of a fatty acid uptake buffer consisting of 0.1% (w/v) BSA in HBSS in addition to 2−100 μM of FFA-SS-luc or Me-FFA-SS-luc. Plates were read immediately, and luminescent images were acquired with a 5-min exposure time back to back for 60 min. All cell-based assays utilized the same kinetic acquisition settings.

Fatty acid uptake assays with HEK293 cells expressing human FATP5 were performed as published by Nie and colleagues.[37] FATP5 expressing cells were seeded into black-wall/clear-bottom 96-well plates and treated with 100 μL of fatty acid uptake buffer including 100 μM FFA-SS-luc, and plates were read immediately.

FFA-SS-Luc Competition Assay. 3T3-luc adipocytes were seeded into black-wall/clear-bottom 96-well plates (Costar) and treated with 100 μL of fatty acid uptake buffer including 20 μM FFA-SS-luc and a titration of 0−2 mM oleate or methyl-oleate immediately prior to imaging.

Enterocyte isolation from FVB-luc+ animals and fatty acid uptake assays with mixed micelles were carried out as previously described for C57BL/6 animals.[28] After isolation, enterocytes were seeded into 96-well plates and treated with fatty acid uptake buffer made with taurocholate instead of BSA in addition to 150 μM FFA-SS-luc and a titration of 0−5 mM oleate or palmitate before imaging.

Insulin-Mediated Uptake of FFA-SS-luc. 3T3-luc adipocytes were seeded into black-wall/clear-bottom 96-well plates (Costar). One group of cells was serum starved in DMEM for 5 h followed by the addition of 100 μL of fatty acid uptake buffer with 20 μM FFA-SS-luc immediately prior to imaging. A second group of cells was treated with DMEM/FBS for 5 h followed by the addition of 100 μL of fatty acid

uptake buffer with 20 μM FFA-SS-luc and 1 μg/mL insulin immediately prior to imaging.

Gavage of FFA-SS-luc and FFA-S-luc. Anesthetized mice received a 50 μL volume gavage of 300 μM FFA-SS-luc or FFA-S-luc (0.01 mg) in a vehicle of 1:1 poly(ethylene glycol) (PEG 400) and propylene glycol (PG). Mice were awake for 5 min postgavage to stimulate peristalsis before they were reanesthetized for imaging. Mice were under constant isoflurane administration in the IVIS Spectrum In Vivo Imager (PerkinElmer, CA), and luminescent images were acquired with a 5-min exposure back to back for 60 min.

Intravenous Injection of FFA-SS-luc and FFA-S-luc. Restrained mice received 100 μL volume tail vein injections of 20 μM FFA-SS-luc or FFA-S-luc (0.0014 mg/mouse) bound to 0.1% (w/v) BSA in PBS. Mice were immediately anesthetized, and luminescent images with a 1-min exposure were acquired.

Intraperitoneal Injection of FFA-SS-luc and FFA-S-luc. Anesthetized mice received a 100 μL volume intraperitoneal injection of 200 μM FFA-SS-luc or FFA-S-luc (0.014 mg/mouse) bound to 0.1% (w/v) BSA in PBS immediately prior to imaging. Luminescent images were acquired with a 3-min exposure back to back for 30 min.

BAT Imaging. Anesthetized mice received 100 μL volume intraperitoneal injection of 200 μM FFA-SS-luc or FFA-S-luc (0.014 mg) immediately prior to imaging. Luminescent images were acquired with a 3-min exposure back to back for 30 min. For BAT activation imaging, mice received intraperitoneal injections of the β-adrenergic stimulator CL316,243 at 1 mg/kg 20 min prior to the FFA-SS-luc injection.

μCT Scans. Mice received a 100 μL volume gavage of 80 mg barium sulfate. After 1 h, mice received a second barium sulfate gavage, immediately followed by a 50 μL volume gavage of 300 μM FFA-SS-luc (0.01 mg) in a vehicle of 1:1 PEG 400 and propylene glycol. Mice were placed in a Mouse Imaging Shuttle Adaptor (Caliper Life Sciences), and luminescent images were acquired with a 5-min exposure back to back for 60 min. Mice were then transferred to the Quantum FX μCT for CT imaging without disruption of position. Co-registration of luminescent and CT images were performed with Living Image software.

Statistical Analysis. Results are reported as mean ± SD and are representative of a series of experiments. Statistical significance was assessed by one-way ANOVA. IC_{50} and all other statistics were analyzed using Prism version 5.0 (Graphpad Software).

■ ASSOCIATED CONTENT

Ⓢ Supporting Information

This material is available free of charge *via* the Internet at http://pubs.acs.org.

■ AUTHOR INFORMATION

Corresponding Author
*E-mail: AStahl@Berkeley.edu.

Author Contributions
¶These authors contributed equally to this work.

Notes
The authors declare no competing financial interest.

■ ACKNOWLEDGMENTS

■ REFERENCES

(1) Wu, Q., Kazantzis, M., Doege, H., Ortegon, A. M., Tsang, B., Falcon, A., and Stahl, A. (2006) Fatty acid transport protein 1 is required for nonshivering thermogenesis in brown adipose tissue. *Diabetes* 55, 3229–3237.

(2) Hull, F. E., Radloff, J. F., and Sweeley, C. C. (1975) Fatty acid oxidation by ischemic myocardium. *Recent Adv. Stud. Card. Struct. Metab.* 8, 153–165.

(3) Drozdowski, L., and Thomson, A. B. (2006) Aging and the intestine. *World J. Gastroenterol.* 12, 7578–7584.

(4) Boden, G., and Shulman, G. I. (2002) Free fatty acids in obesity and type 2 diabetes: defining their role in the development of insulin resistance and beta-cell dysfunction. *Eur. J. Clin. Invest.* 32 (Suppl 3), 14–23.

(5) Chiu, H. C., Kovacs, A., Blanton, R. M., Han, X., Courtois, M., Weinheimer, C. J., Yamada, K. A., Brunet, S., Xu, H., Nerbonne, J. M., Welch, M. J., Fettig, N. M., Sharp, T. L., Sambandam, N., Olson, K. M., Ory, D. S., and Schaffer, J. E. (2005) Transgenic expression of fatty acid transport protein 1 in the heart causes lipotoxic cardiomyopathy. *Circ. Res.* 96, 225–233.

(6) Fabbrini, E., Sullivan, S., and Klein, S. (2010) Obesity and nonalcoholic fatty liver disease: biochemical, metabolic, and clinical implications. *Hepatology* 51, 679–689.

(7) Chiu, H. C., Kovacs, A., Ford, D. A., Hsu, F. F., Garcia, R., Herrero, P., Saffitz, J. E., and Schaffer, J. E. (2001) A novel mouse model of lipotoxic cardiomyopathy. *J. Clin. Invest.* 107, 813–822.

(8) Trauner, M., Arrese, M., and Wagner, M. (2010) Fatty liver and lipotoxicity. *Biochim. Biophys. Acta* 1801, 299–310.

(9) Lee, Y., Hirose, H., Ohneda, M., Johnson, J. H., McGarry, J. D., and Unger, R. H. (1994) Beta-cell lipotoxicity in the pathogenesis of non-insulin-dependent diabetes mellitus of obese rats: impairment in adipocyte-beta-cell relationships. *Proc. Natl. Acad. Sci. U.S.A.* 91, 10878–10882.

(10) Hauner, H. (2002) The mode of action of thiazolidinediones. *Diabetes Metab. Res. Rev.* 18 (Suppl2), S10–15.

(11) Keating, G. M., and Jarvis, B. (2001) Orlistat: in the prevention and treatment of type 2 diabetes mellitus. *Drugs* 61, 2107–2119 ; discussion pp 2120–2121.

(12) Carvalho, R. A., Sousa, R. P., Cadete, V. J., Lopaschuk, G. D., Palmeira, C. M., Bjork, J. A., and Wallace, K. B. (2010) Metabolic remodeling associated with subchronic doxorubicin cardiomyopathy. *Toxicology* 270, 92–98.

(13) Yoshinaga, K., and Tamaki, N. (2007) Imaging myocardial metabolism. *Curr. Opin. Biotechnol.* 18, 52–59.

(14) Gropler, R. J., Beanlands, R. S., Dilsizian, V., Lewandowski, E. D., Villanueva, F. S., and Ziadi, M. C. (2010) Imaging myocardial metabolic remodeling. *J. Nucl. Med.* 51 (Suppl 1), 88S–101S.

(15) Niot, I., Poirier, H., Tran, T. T., and Besnard, P. (2009) Intestinal absorption of long-chain fatty acids: evidence and uncertainties. *Prog. Lipid Res.* 48, 101–115.

(16) Schulz, G., von Dahl, J., Kaiser, H. J., Koch, K. C., Sabri, O., Banneitz, L., Cremerius, U., and Buell, U. (1996) Imaging of beta-oxidation by static PET with 14(R,S)-[18F]-fluoro-6-thiaheptadecanoic acid (FTHA) in patients with advanced coronary heart disease: a comparison with 18FDG-PET and 99Tcm-MIBI SPET. *Nucl. Med. Commun.* 17, 1057–1064.

(17) DeGrado, T. R., Wang, S., Holden, J. E., Nickles, R. J., Taylor, M., and Stone, C. K. (2000) Synthesis and preliminary evaluation of (18)F-labeled 4-thia palmitate as a PET tracer of myocardial fatty acid oxidation. *Nucl. Med. Biol.* 27, 221–231.

(18) Massoud, T. F., and Gambhir, S. S. (2003) Molecular imaging in living subjects: seeing fundamental biological processes in a new light. *Genes Dev.* 17, 545–580.

(19) Prescher, J. A., and Contag, C. H. (2010) Guided by the light: visualizing biomolecular processes in living animals with bioluminescence. *Curr. Opin. Chem. Biol.* 14, 80–89.

(20) McCaffrey, A., Kay, M. A., and Contag, C. H. (2003) Advancing molecular therapies through in vivo bioluminescent imaging. *Mol. Imaging* 2, 75–86.

(21) Gheysens, O., and Mottaghy, F. M. (2009) Method of bioluminescence imaging for molecular imaging of physiological and pathological processes. *Methods* 48, 139–145.

(22) Shah, K., Tung, C. H., Breakefield, X. O., and Weissleder, R. (2005) In vivo imaging of S-TRAIL-mediated tumor regression and apoptosis. *Mol. Ther.* 11, 926–931.

(23) Liu, J. J., Wang, W., Dicker, D. T., and El-Deiry, W. S. (2005) Bioluminescent imaging of TRAIL-induced apoptosis through detection of caspase activation following cleavage of DEVD-amino-luciferin. *Cancer Biol. Ther.* 4, 885–892.

(24) Yao, H., So, M. K., and Rao, J. (2007) A bioluminogenic substrate for in vivo imaging of beta-lactamase activity. *Angew. Chem., Int. Ed.* 46, 7031–7034.

(25) Dragulescu-Andrasi, A., Liang, G., and Rao, J. (2009) In vivo bioluminescence imaging of furin activity in breast cancer cells using bioluminogenic substrates. *Bioconjugate Chem.* 20, 1660–1666.

(26) Wehrman, T. S., von Degenfeld, G., Krutzik, P. O., Nolan, G. P., and Blau, H. M. (2006) Luminescent imaging of beta-galactosidase activity in living subjects using sequential reporter-enzyme luminescence. *Nat. Methods* 3, 295–301.

(27) Van de Bittner, G. C., Dubikovskaya, E. A., Bertozzi, C. R., and Chang, C. J. (2010) In vivo imaging of hydrogen peroxide production in a murine tumor model with a chemoselective bioluminescent reporter. *Proc. Natl. Acad. Sci. U.S.A.* 107, 21316–21321.

(28) Stahl, A., Hirsch, D. J., Gimeno, R. E., Punreddy, S., Ge, P., Watson, N., Patel, S., Kotler, M., Raimondi, A., Tartaglia, L. A., and Lodish, H. F. (1999) Identification of the major intestinal fatty acid transport protein. *Mol. Cell* 4, 299–308.

(29) Dubikovskaya, E. A., Thorne, S. H., Pillow, T. H., Contag, C. H., and Wender, P. A. (2008) Overcoming multidrug resistance of small-molecule therapeutics through conjugation with releasable octaarginine transporters. *Proc. Natl. Acad. Sci. U.S.A.* 105, 12128–12133.

(30) Jones, L. R., Goun, E. A., Shinde, R., Rothbard, J. B., Contag, C. H., and Wender, P. A. (2006) Releasable luciferin-transporter conjugates: tools for the real-time analysis of cellular uptake and release. *J. Am. Chem. Soc.* 128, 6526–6527.

(31) Wender, P. A., Goun, E. A., Jones, L. R., Pillow, T. H., Rothbard, J. B., Shinde, R., and Contag, C. H. (2007) Real-time analysis of uptake and bioactivatable cleavage of luciferin-transporter conjugates in transgenic reporter mice. *Proc. Natl. Acad. Sci. U.S.A.* 104, 10340–10345.

(32) Denburg, J. L., Lee, R. T., and McElroy, W. D. (1969) Substrate-binding properties of firefly luciferase. *Arch. Biochem. Biophys.* 134, 381–394.

(33) Jenkins, D. E., Oei, Y., Hornig, Y. S., Yu, S., Dusich, J., Purchio, T., and Contag, P. R. (2003) Bioluminescent imaging (BLI) to improve and refine traditional murine models of tumor growth and metastasis. *Clin. Exp. Metastasis* 20, 733–744.

(34) Schaffer, J. E., and Lodish, H. F. (1994) Expression cloning and characterization of a novel adipocyte long chain fatty acid transport protein. *Cell* 79, 427–436.

(35) Cao, Y. A., Wagers, A. J., Beilhack, A., Dusich, J., Bachmann, M. H., Negrin, R. S., Weissman, I. L., and Contag, C. H. (2004) Shifting foci of hematopoiesis during reconstitution from single stem cells. *Proc. Natl. Acad. Sci. U.S.A.* 101, 221–226.

(36) Kazantzis, M., and Stahl, A. (2012) Fatty acid transport proteins, implications in physiology and disease. *Biochim. Biophys. Acta* 1821, 852–857.

(37) Nie, B., Park, H. M., Kazantzis, M., Lin, M., Henkin, A., Ng, S., Song, S., Chen, Y., Tran, H., Lai, R., Her, C., Maher, J. J., Forman, B. M., and Stahl, A. (2012) Specific bile acids inhibit hepatic fatty acid uptake. *Hepatology.*, DOI: 10.1002/hep.25797.

(38) Wu, Q., Ortegon, A. M., Tsang, B., Doege, H., Feingold, K. R., and Stahl, A. (2006) FATP1 is an insulin-sensitive fatty acid transporter involved in diet-induced obesity. *Mol. Cell. Biol.* 26, 3455–3467.

(39) Stahl, A., Evans, J. G., Pattel, S., Hirsch, D., and Lodish, H. F. (2002) Insulin causes fatty acid transport protein translocation and enhanced fatty acid uptake in adipocytes. *Dev. Cell* 2, 477–488.

(40) Kuo, C., Coquoz, O., Troy, T. L., Xu, H., and Rice, B. W. (2007) Three-dimensional reconstruction of in vivo bioluminescent sources based on multispectral imaging. *J. Biomed. Opt. 12*, 024007.

(41) Goodman, B. E. (2010) Insights into digestion and absorption of major nutrients in humans. *Adv. Physiol. Educ. 34*, 44−53.

(42) Hirasawa, A., Tsumaya, K., Awaji, T., Katsuma, S., Adachi, T., Yamada, M., Sugimoto, Y., Miyazaki, S., and Tsujimoto, G. (2005) Free fatty acids regulate gut incretin glucagon-like peptide-1 secretion through GPR120. *Nat. Med. 11*, 90−94.

(43) Emken, E. A. (2001) Stable isotope approaches, applications, and issues related to polyunsaturated fatty acid metabolism studies. *Lipids 36*, 965−973.

(44) Tran, T. T., and Kahn, C. R. (2010) Transplantation of adipose tissue and stem cells: role in metabolism and disease. *Nat. Rev. Endocrinol. 6*, 195−213.

(45) Baldini, G., Hohl, T., Lin, H. Y., and Lodish, H. F. (1992) Cloning of a Rab3 isotype predominantly expressed in adipocytes. *Proc. Natl. Acad. Sci. U.S.A. 89*, 5049−5052.

■ NOTE ADDED AFTER ASAP PUBLICATION

This paper was published ASAP on September 6, 2012. The legends for Figure 1 and Figure 4 and the Acknowledgments have been updated. The revised version was posted on October 1, 2012.